(M,N) codoping (M = Nb or Ta) and CoO nanoparticle decoration of TiO2 nanotubes: synergistic enhancement of visible photoelectrochemical water splitting

Thomas Favet, Sharmin Sharna, Valérie Keller, My Ali El Khakani, Thomas Cottineau

(M,N) codoping (M = Nb or Ta) and CoO nanoparticle decoration of TiO_2 nanotubes: synergistic enhancement of visible photoelectrochemical water splitting

Thomas Favet, Sharmin Sharna, Valérie Keller, My Ali El Khakani and Thomas Cottineau**

T. Favet, V. Keller, T. Cottineau:
Institut de Chimie et Procédés pour l'Énergie, l'Environnement et la Santé, (ICPEES UMR7515) - CNRS - Université de Strasbourg, 25 rue Becquerel, 67087 Strasbourg, France.
T. Favet, M.A. El Khakani:
Institut National de Recherche Scientifique - Centre Energie, Matériaux et Télécommunication (INRS-EMT) 1650, boulevard Lionel-Boulet Varennes (Québec) J3X 1S2 Canada
S. Sharna:
Institut de Physique, Chimie et Matériaux de Strasbourg, (IPCMS UMR 7504) - CNRS - Université de Strasbourg, 23 rue du Loess, 67034 Strasbourg, France.

*Corresponding authors: cottineau@unistra.fr
m.a.elkhakani@inrs.ca

Abstract:

The (M,N) codoping of TiO_2 and the formation of heterojunctions by association with co-catalyst nanoparticles are two approaches that can improve the efficiency of TiO_2 used as photoanodes for PEC water splitting. In this study, reactive pulsed laser deposition (PLD) of CoO nanoparticles on the surface of (M,N)-codoped TiO_2 nanotubes has been used to combine these two methods. The (M,N) codoping reduced the band gap of TiO_2 nanotubes and the subsequent nanodecoration significantly increased the photocurrent production under simulated sunlight and visible light conditions. The most significant improvement was obtained for (Nb,N) TiO_2-NTs decorated with CoO-NPs, which showed a factor of 3 increase, and a significant contribution from the visible part of the spectrum, which accounts for 40% of the photocurrent generated in this sample. Our results suggest that this enhancement is due

to a synergistic effect between the (M,N) codoping of TiO_2-NTs and the presence of CoO-NPs through the formation of a high density of local triple phase interfaces (TPI) (n-TiO_2/p-CoO/electrolyte). A modification of the band energy structure at these TPIs allows better extraction of charge carriers generated by visible light in (M,N) TiO_2-NTs thanks to the presence of CoO nanoparticles.

Keywords: Photoelectrochemistry, TiO_2 nanotubes, Pulsed laser deposition, cobalt oxide nanoparticles, OER catalyst, water splitting.

1. Introduction

Hydrogen is a promising fuel for heavy transportation and to reduce the carbon footprint of heavy industries.[1] Most of the H_2 produced so far relies mainly on steam reforming of methane, which produces a large amount of CO_2, and it is urgent to develop greener approaches for H_2 production, such as direct water splitting using renewable primary energy sources.[2] Photo-electrochemical (PEC) and photocatalytic (PC) water-splitting are promising approaches for the direct conversion of abundant solar energy into clean H_2.[3] Nevertheless, the efficiency and stability of these approaches need to be improved to demonstrate their economic viability.[4] To ensure efficient solar-to-chemical energy conversion, photo-active devices must absorb a large portion of the solar spectrum, present good charge carrier transport properties, and have high catalytic activity while being stable in water.[5,6] So far, no material can meet all these criteria, and the formation of novel heterostructures through the combination of several materials, each designed to perform a specific function in the reaction, increases the chances of meeting these requirements.[7–9] For instance, heterojunctions between the SC and co-catalyst nanoparticles (NPs) will assure a more efficient charge transfer for one of the half-reactions (Hydrogen or Oxygen Evolution Reactions; HER or OER).[6] The heterojunction between the SC and the co-catalyst also provides a built-in electric field inside the heteronanostructure which acts as a driving force for charge carriers separation.[10] In this perspective of forming heterostructures with enhanced properties for PEC, this work proposes, for the first time, the rationale association of recent advances in the field of SC materials for PEC: (M,A) codoping of TiO_2 nanotubes (M= metal cation; A = anion) and their decoration by PLD with non-noble metal co-catalyst.

The codoping of TiO_2 has been first proposed from DFT calculation, as a way to redshift the light absorption of TiO_2.[11,12] This strategy combines the substitution of Ti^{4+} by a transition metal cation $M^{(4+n)+}$ with the substitution of O^{2-} by an anion $A^{(2+p)-}$.[13] While

mono-doping approaches, such as N doping of TiO_2, allow visible light absorption, the photoconversion efficiency and stability remain limited due to the creation of defects such as oxygen vacancies to compensate for the charge introduced by N^{3-}.[14,15] Achieving passivated codoping of TiO_2 material (also referred to as coalloying),[16] with a stoichiometric charge balance between A and M, according to equation 1, should lead to a more stable structure with fewer defects acting as charge recombination centers.

$$Ti_{(1-x)}^{4+} M_x^{(4+n)+} O_{\left(2-\frac{n}{p}x\right)}^{2-} A_{\frac{n}{p}x}^{(2+p)-} \qquad \text{(eq. 1)}$$

As a consequence, a large number of heteroatoms can be introduced into the lattice of TiO_2 and result in the hybridization between *p* and *d* orbitals of the doping species and the orbitals of TiO_2 to form a continuum of energy above the valence band that lowers the band gap.[13] To date, few studies have reported the synthesis of codoped TiO_2 materials.[17–24] Significant improvements in visible light absorption have been reported, although the stoichiometric balance of the charges as defined in eq. 1 has never been reported, probably due to the predominance of intrinsic defects of TiO_2.[25] Our group was the first to apply (M,N) codoping to aligned TiO_2-NTs which resulted in a 3-fold higher visible light PEC activity ($\lambda > 400$ nm) and better stability than its N-doped counterpart.[19,22]

On the other side, the nanodecoration of photoelectrodes with co-catalysts was proposed to reduce the overpotential of the OER, which is a complex reaction involving 4-electron transfer with slow kinetics.[26] Among the possible co-catalysts, IrO_2 and RuO_2 have been identified as state-of-the-art candidates,[27] but their cost limits their application. Cobalt- and nickel-based materials have proven to be among the most promising non-noble metal co-catalysts to enhance the OER efficiency while being stable in alkaline electrolytes.[28,29] Heterostructures associating electrodeposited CoO_x NPs and TiO_2-NTs were found to double the photocurrent compared to bare TiO_2-NTs.[30] Nickel oxide NPs were also electrodeposited onto TiO_2-NTs electrode and found to double the efficiency of

photocatalytic degradation of 4-chlorophenol.[31] These improved activities were ascribed to better charge separation at the TiO_2/NiO interface. Recently, we have demonstrated the potential of pulse laser deposition (PLD) for the deposition of NiCo, CoO, and NiO NPs onto TiO_2-NTs arrays for PEC splitting.[32,33] The PLD is a non-equilibrium physical technique that has been proven to be very effective in depositing high-purity crystalline materials NPs with strong adhesion to the substrate.[34–37] In our previous results, two main factors explain the enhanced PEC performance after CoO NPs deposition: firstly, a more favorable interfacial electronic band structure at the p-n CoO/TiO_2 heterojunction allows a better separation of charge carriers compared to the NiO/TiO_2 system. Secondly, with a bandgap of ~2.5 eV, CoO can harvest visible photons ($\lambda < 500$ nm) and convert them into charge carriers.

While (M,A) codoping of TiO_2 and the decoration of TiO_2-NTs by CoO-NPs have been proven to individually improve the performance of the photoelectrodes, we propose in the present study to capitalize on the combination of both approaches to achieve (M,N) codoped TiO_2-NTs decorated with CoO-NPs. These novel heterostructures are investigated to determine the contribution of each component to the overall efficiency of the photoanode for the PEC water-splitting. By combining spectroscopic and PEC experiments, we aim to determine whether we can benefit from a synergistic effect or the additional contributions of (M.N)-codoping and CoO-NPs-decoration. Our results indicate that, for optimal conditions, the PEC performance of CoO-NPs and (M,N) codoped modified TiO_2-NTs has more than tripled compared to their bare TiO_2-NTs counterparts while keeping stable performances for more than 35h. Due to the improved separation of charge carriers from absorbed visible light photons, the synergistic effect is particularly pronounced in the visible light region. Consequently, CoO-NPs decorated (Nb,N) TiO_2-NTs were found to produce as much H_2 and O_2 using only visible light ($\lambda > 400$ nm), as bare-TiO_2-NTs electrodes under full solar spectra.

2. Material and methods

2.1. Codoped TiO_2-NTs synthesis and decoration

Undoped and M-doped TiO_2-NTs (M = Nb or Ta) were synthesized by anodization from titanium, Nb-Ti or Ta-Ti alloy foils ([M] = $5\%_{at.}$). The metallic foils were cleaned by ultrasonication in acetone, ethanol and ultra-pure water successively and used as an anode in a 2 electrodes cell. The electrolyte was composed of ethylene glycol, $0.3\%_{w/w}$ of NH_4F, and $1\%_{v/v}$ of ultra-pure water. The synthesis of the nanotubes was performed by applying 45V with a Bio-Logic SP300 potentiostat until a charge density of 5 $C.cm^{-2}$ was reached. The electrodes were then thoroughly rinsed with ultra-pure water. To incorporate N atoms into the (M,N) TiO_2-NTs samples, a post-anodization thermal treatment was performed at 500°C in NH_3 at 500°C for 12h (details of the synthesis and annealing process can be found in ESI).

The deposition of CoO NPs on the undoped or (M,N) codoped TiO_2-NTs was performed through the pulsed laser (248 nm KrF laser) ablation of a cobalt metallic target under a partial pressure of 300 mTorr of oxygen, which is placed parallel to the samples holder. Before each CoO-NPs deposition, the target was systematically cleaned by ablating its surface for 5 min. The number of laser pulses (N_{LP}) was adjusted to vary the CoO-NPs loading (N_{LPs} = 500, 2000, 3500, 5000, 7500, or10000).

2.2. Characterization methods

The surface composition of the photoelectrodes was studied by X-Ray Photoelectron Spectroscopy (XPS Thermo VG Scientific). The morphology of our samples was examined using SEM (Gemini-SEM 500; Zeiss) and TEM (JEOL JEM-2100F) equipped with EDS elemental analysis. X-ray diffraction patterns were measured using a Bruker D8 diffractometer equipped with a LynxEye PSD detector. The UV-vis optical properties were characterized by using a Perkin-Elmer Lambda 950 spectrometer equipped with a 100 mm integration sphere. Photo-electrochemical measurements were performed in a 3-electrode cell,

filled with 100 mL of electrolyte (0.01 M NaOH + 0.1 M Na_2SO_4). This cell was composed of 2 compartments: one with a platinum mesh acting as a counter electrode and one with the photoanode and the reference mercury sulfate electrode ((MSE; E = 0.64 + 0.059 × pH V vs RHE). Cyclic voltammetry (CV) measurements were performed at a scan rate of 10 $mV.s^{-1}$ between -1.3 and -0.1 V vs. MSE under simulated solar light irradiation (AM1.5G filtered Xe arc lamp; 100 $mW.cm^{-2}$). A 400 nm long pass filter was added between the lamp and the cell to measure the efficiency under visible light only (70 $mW.cm^{-2}$). The external quantum efficiency (EQE) was measured between 280 and 800 nm by a Newport 1/8 Cornerstone monochromator at an applied potential of 1.15 V vs. RHE. The stability of the photoanodes was investigated for at least 35 h in chronoamperometry at 1.05 V vs RHE under UV irradiation (365 nm LED; 7.5 $mW.cm^{-2}$). The gas production was determined with a micro gas chromatograph (µ-GC; SRA Instrument R-3000) connected to the PEC cell. For O_2 detection, a 14m column (He carrier gas) was used, whereas a 30m column was used to measure the H_2 produced (Ar carrier gas). During the experiment, a bias of 1.15 V vs RHE was applied and the samples were irradiated with either AM1.5G simulated solar light or visible light and nitrogen was used as carrier gas. Acquisition of the chromatograms was performed with an injection time of 50 ms at 90°C every 3 minutes.

3. Results and discussion

3.1.Photoelectrodes characterizations

Typical SEM images of the annealed (Nb,N) and (Ta,N) codoped TiO_2-NTs are presented in **Figure 1.a & 1.b**, respectively. Their dimensions averaged on 10 measurements at different positions on the electrode, are 4.05 ± 0.15 µm in length, 110 ± 10 and 50 ± 10 nm in external and internal diameter, respectively. These values are comparable to those of undoped TiO_2-NTs grown from titanium foil with the same anodization parameters.[38] This

control of the growth of NTs was achieved by limiting the anodization reaction to a given charge instead of a time. Indeed, the charge transferred can be directly related to the quantity of metal oxide formed by electrochemical anodization, independently of the synthesis parameters, and consequently, it gives a reliable indicator of the film thickness.

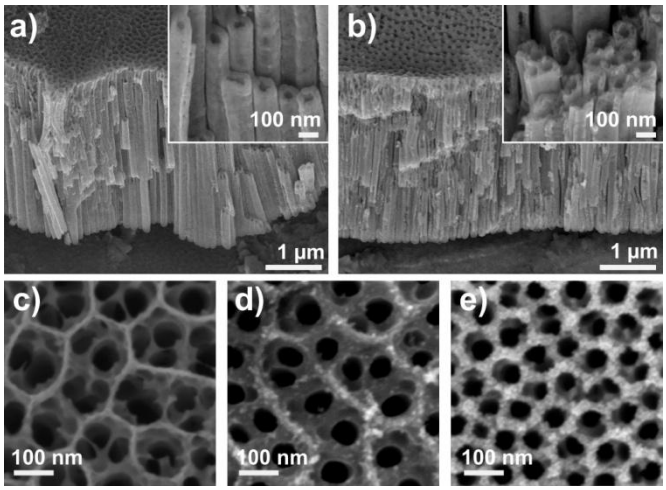

***Figure 1: (a)** and **(b)** are the respective SEM images of (Nb,N) and (Ta,N) codoped TiO_2-NTs (observation with a tilt of 45°; insets are magnifications on the nanotubes opening). The bottom-line images are top-view SEM images of the (Nb,N) TiO_2-NTs surface before **(c)**, and after their PLD-nanodecoration with CoO-NPs at N_{LP}=2000 **(d)** and N_{LP} =10000 **(e)**.*

Figures 1.c, 1.d & 1.e are representative top views of the (Nb,N) TiO_2-NTs samples before and after their decoration with CoO-NPs at 2000 and 10000 N_{LP}. The thin honeycomb structure at the top of the TiO_2-NTs film is a residual of the initiation layer left by the pre-anodization step. The openings of the NTs, with an inner diameter of ~50 nm, can be observed below. Comparing the top-view SEM images of the NTs before (**fig. 1.c**) and after their decoration with CoO (**fig. 1.d&e**) reveals the presence of the PLD-deposited CoO-NPs appearing brighter on the edges of the nanotube walls. As the N_{LP} is increased from 2000 to 10000, the density of NPs on the NTs surface significantly increases with a tendency to agglomerate and covers completely the top edges of the NTs. To determine precisely the size of the CoO-NPs, we gently scratched the surface of the electrodes and observed the detached materials by TEM. **Figure 2.a** shows a TEM image of a bunch of aligned TiO_2-NTs and

Figure 2.b is a magnification on the top part of the TiO_2-NTs, where a high concentration of CoO-NPs is expected according to the SEM images. On **fig. 2.b,** one can distinguish two types of nanostructures: (i) relatively large features (bottom and left) which correspond to the TiO_2 crystallites constituting the NTs; and (ii) small particles (center-right of the image) with a size of ~5 nm which correspond to CoO-NPs. This particle size, consistent with our previous results done on CoNi-NPs,[32] explains why no X-ray diffraction peaks associated with any cobalt or cobalt oxide phases were observed on these samples. Indeed, according to the Scherrer equation, such a size should result in peaks with an FWHM of around 2° and given the small volume of these NPs compared to the volume of TiO_2, these peaks would not be observable by XRD. To further ascertain the crystalline characteristic of these NPs, high-resolution-TEM (HRTEM) was conducted (**Fig. 2.c**) and after FFT filtering, to enhance the contrast in some areas, distances between the atomic plans were calculated. For the largest particles (left square in Fig 2.c), an average distance of 3.5 ± 0.1 Å was measured and for the smallest ones located at the surface, this distance was found to be 2.5 Å or 2.1 ± 0.1 Å. These values could correspond to TiO_2 anatase (101), CoO (111) and CoO (200) plans, respectively (more images available in **Fig. S3.a & b**). To determine the spatial distribution of CoO co-catalyst in the NTs film, STEM EDS mapping was done for (Ta,N) TiO_2-NTs sample after deposition of 10000 N_{LP} of CoO. **Figure 2.d** presents the composite image of the different elements for a bunch of NTs with Ti, Ta and Co in red, blue and green respectively (more images are available in **ESI figures S1, S2, S3**). An accumulation of cobalt can be observed at the top of the NTs array. In square 1 at the top of the nanotube film (**figure 2.e)** the atomic ratio of cobalt, titanium, and tantalum are 8, 87 and 5 % respectively, while in the other part of the nanotube array, this ratio decreases below 1% (square 2 & 3). It should be noted that an overestimation of Co concentration is likely to come from the secondary X-ray (fluorescence) due to the presence of Tantalum which has a high atomic number. Nevertheless, the result of

this EDS mapping confirmed the presence of Co NPs all along the NTs with a more important density on the top-side of the NTs array, in agreement with our previous works on PLD of Co, Ni and CoNi NPs on TiO_2-NTs.[32,33]

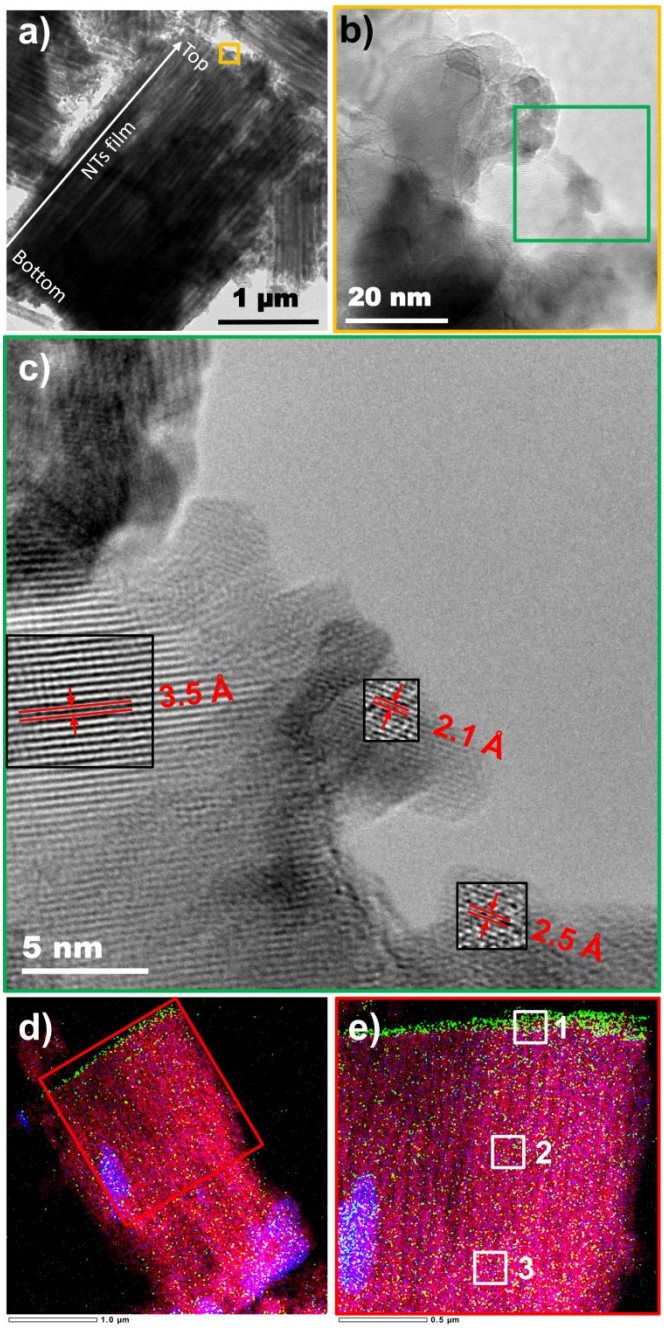

Figure 2: *TEM images of TiO_2-NTs after their decoration with CoO-NPs at N_{LP} = 10000:* ***(a)*** *whole nanotubes (orientation given by the white arrow);* ***(b)*** *zoomed TEM image of the top part of the NTs array (yellow square on fig. 2.a); and* ***(c)*** *HRTEM of the green squared zone in (b).* ***(d)*** *STEM EDS mapping of a bunch of detached (Ta,N) TiO_2-NTs decorated 10000 N_{LP} of CoO (Ti, Ta and Co are represented in red, blue and green respectively; more details in ESI);* ***(e)*** *zoomed mapping on the upper part of the NTs bunch in figure 2.d.*

The XPS spectra of (Nb,N) and (Ta,N) codoped samples after CoO-NPs deposition at N_{LP} = 10000 are presented in **Figure 3**. The presence of cobalt was confirmed by SEM and TEM EDS, but more information about the nature of the co-catalyst was obtained by the XPS of Co 2p region presented in **Figure 3.a.** Both samples display a doublet Co $2p_{3/2}$ and $2p_{1/2}$ with respective binding energies of 780.4 and 795.1 ± 0.2 eV. The binding energies of this doublet along with its energy split (ΔE=14.7 eV) are very consistent with Co^{2+} in CoO.[39]. The Co 2p doublet is also associated with two satellite peaks, whose shapes are characteristic of Co^{2+}, at 785.7 and 803.7 ± 0.2 eV. These XPS results along with EDS and HRTEM indicate that the nanoparticles formed during the PLD process consist of the CoO phase. The XPS spectra of Ti 2p, O 1s and C 1s (ESI **Figure S5**) are typical for TiO_2-NTs with binding energy for the doublet Ti $2p_{3/2}$ & $2p_{1/2}$ characteristic of Ti^{4+} in TiO_2.[40] Similarly, the Nb 3d and Ta 4d core level spectrum (**Figure S4.b & c**) are characteristic of Nb^{5+} and Ta^{5+}.[41] In the binding energy range around 400 eV, besides a broad contribution of Ta $4p_{3/2}$ (404.4 eV; **Fig. 3.b**) 2 peaks of nitrogen, labeled N $1s_i$ and N $1s_s$, are observed at 400.1 and 396.2 ± 0.2 eV and are attributed to interstitial and substitutional nitrogen, respectively. The N/M surface concentration ratios determined by XPS are 0.3 for (Nb,N) and 0.4 for (Ta,N) codoped TiO_2-NTs samples, suggesting a non-complete charge compensation between anionic and cationic doping elements contrary to the ideal case expected from eq. 1. Nevertheless, XPS is a shallow surface method and a surface enrichment of doping cations cannot be excluded. In order, to confirm the presence of Nb or Ta cations in the TiO_2 lattice, Le Bail profile matching was performed on the XRD patterns of the nanotube samples (ESI **Figure S6** and **Table S1**). The results confirm a lattice volume increase for TiO_2 anatase of 0.44 and 0.64% for (Nb,N) and (Ta,N) codoped samples in comparison with the undoped TiO_2.

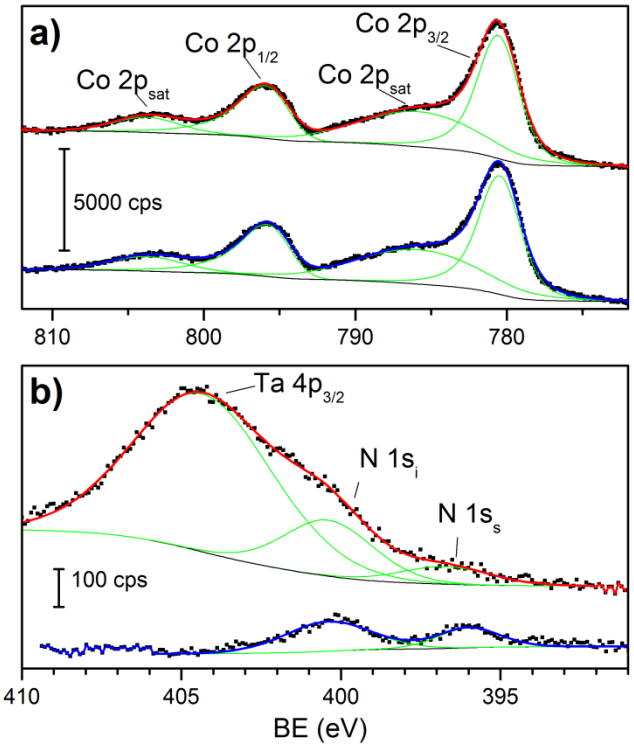

Figure 3: *high-resolution XPS spectra of Co 2p* ***(a)*** *and N 1s* ***(b)*** *core levels of (Nb,N) and (Ta,N) TiO_2-NTs after their PLD decoration with CoO-NPs (at N_{LP}= 10000).*

The optical properties of the TiO_2-based nanotubes were measured by UV visible spectroscopy in transmission mode after removing the nanotube film from the metal substrate, using a procedure detailed elsewhere.[42] A part of this film is then immobilized between two quartz slides and installed at the entrance port of an integrating sphere. The normalized UV-visible spectra of the doped and pristine TiO_2-NTs samples are presented in **Figure 4.a**. All the samples exhibit an exponential background in the visible region which is attributed to light diffusion on the particles constituting the film immobilized between the glass slides. The undoped TiO_2-NTs and the cationic doped samples present an absorption edge starting at ~400 nm, while both (Ta,N) and (Nb,N) codoped samples are found to exhibit a second absorption edge around 500 nm. It should be noted that the two absorption edges observed in these codoped materials suggest the presence of two domains in the samples with different optoelectronic properties. Presumably, this is due to nitrogen diffusion limitation during the

nitridation process: the N doping may occur less efficiently at the closed bottom of the nanotube (metal foil/oxide-NTs interface) where the NTs walls are thicker.[43] The apparent band gap (E_G) associated with these optical transitions was calculated by extrapolating the linear part on the Tauc plots (**Figure 4.b**) according to the Tauc equation:

$$Abs = a\frac{(h\nu - E_G)^m}{h\nu} \qquad \text{(eq. 2)}$$

For an indirect bandgap material, like TiO_2 anatase, m = 2, and a is an experimental constant. For undoped and Ta or Nb-doped samples, a single transition is observed between 3.0 and 3.1 eV. This value is consistent with the bandgap of anatase TiO_2 and no significant change of band gap was expected for Nb and Ta doped TiO_2 since the energy of the d orbitals of Nb and Ta is close to the one of Ti 3d orbitals that constitute the conduction band of TiO_2.[12] For the codoped samples, the first absorption edge is found to be associated with a bandgap of 2.4-2.5 eV, resulting in light absorption in the visible part of the solar spectrum that is brought by N 2p orbitals whose energy is above the valence band of TiO_2.[44]

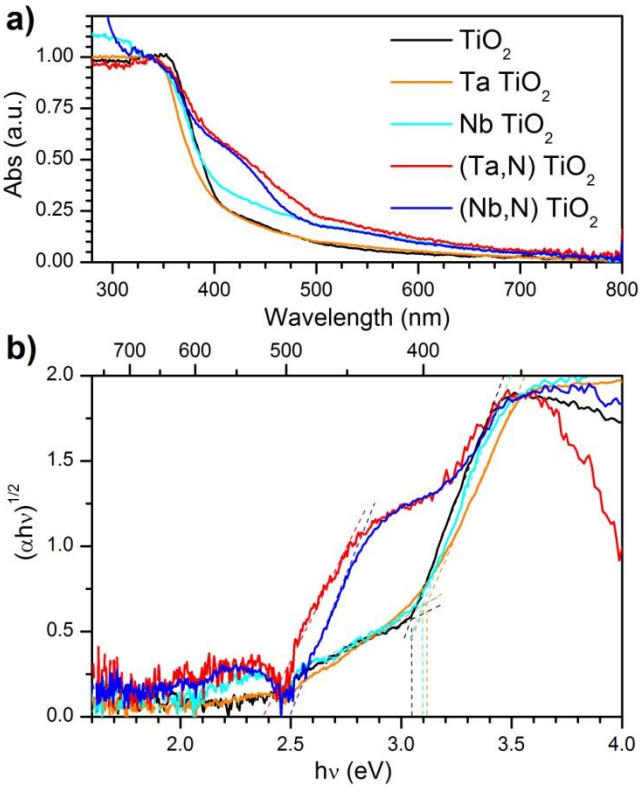

Figure 4: (a) *UV visible absorbance spectra of the pristine, cation doped and codoped TiO_2-NTs samples recorded in transmission mode.* ***(b)*** *The corresponding Tauc plots after diffusive background subtraction.*

3.2.Photo-electrochemical measurements

Cyclic voltammetry (CV) experiments were conducted for each sample in the dark and under illumination with either simulated AM1.5G solar light or only visible light ($\lambda > 400$ nm). The photocurrents ($J_{AM1.5}$ and J_{vis}) are then calculated by subtracting the current from the CV in the dark from the current obtained under AM1.5G or visible light. **Figure 5** presents the $J_{AM1.5}$ and J_{vis} photocurrents for the (Nb,N) and (Ta,N) codoped TiO_2-NTs samples exhibiting the highest performance before and after CoO-NPs decoration. The optimal nanodecoration conditions were found to be N_{LP} = 2000 for the undoped TiO_2-NTs,[33] while N_{LP} = 10000 yielded the highest photocurrent in the case of (M,N) codoped TiO_2-NTs. The main results in terms of photocurrent densities (under both AM1.5G and visible light) of the three photoelectrodes as well as the visible light contribution to their total photocurrent are gathered in **Table 1**. Before CoO-NPs decoration, all samples present a maximal photocurrent within the range 0.12-0.16 $mA.cm^{-2}$ at 1.0V vs RHE under AM1.5G irradiation while under visible light (dashed lines), a clear difference can be observed between the undoped-TiO_2 and the (M,N) codoped samples. For TiO_2, J_{vis} is limited to only 0.005 $mA.cm^{-2}$, whereas for (M,N) codoped samples it reaches approximately 0.020 $mA.cm^{-2}$. In other words, more than 15% of the overall photocurrent came from visible photons conversion for (M,N) codoped samples, while it is only 3.6% for TiO_2-NTs electrodes. This is in line with the UV-Vis spectroscopy results that show a redshift of light absorption for the (M,N) TiO_2-NTs and it confirms that this visible light absorption results in useful photon-to-electron conversion.

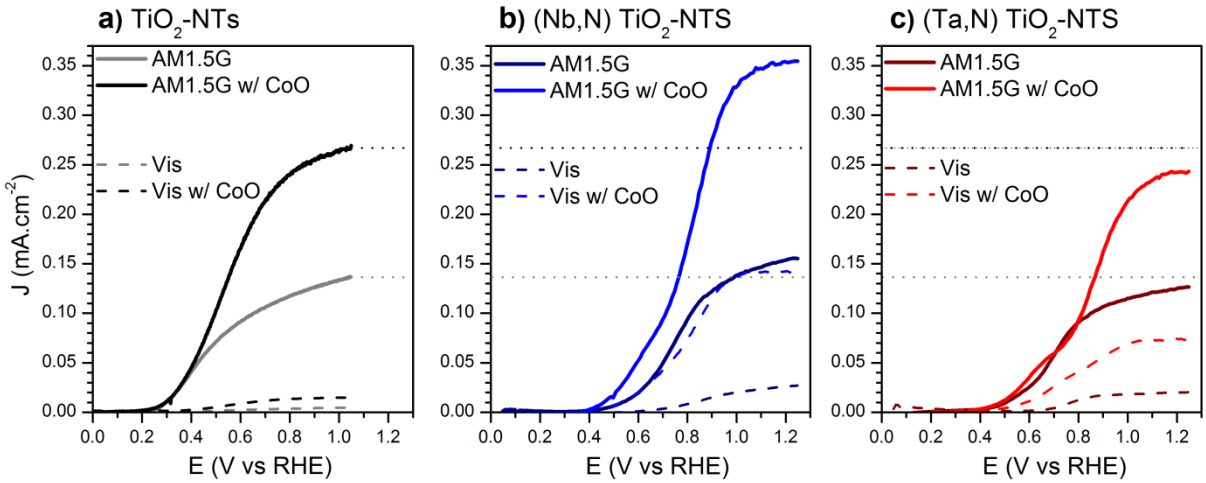

Figure 5: *Photocurrents obtained by cyclic voltammetry in 0.01 mol.L^{-1} NaOH and 0.1 mol.L^{-1} Na_2SO_4 electrolyte under AM1.5G simulated solar light (solid lines) or visible light (dashed lines) for different photoanodes before and after their decoration with CoO-NPs:* ***(a)*** *undoped-TiO_2-NTs (CoO deposition at N_{LP} = 2000);* ***(b)*** *(Nb,N) TiO_2-NTs and* ***(c)*** *(Ta,N) TiO_2-NTs (CoO deposition at N_{LP}= 10000). The horizontal dotted lines indicate the photocurrent of TiO_2-NTs as a guideline for comparison.*

After CoO-NPs nanodecoration, different PEC behaviors depending on the nature of its underlying SC electrode are observed. For undoped-TiO_2-NTs, the CoO-NPs decoration is found to double the photocurrent under solar irradiation from 137 to 269 µA.cm^{-2} and also to increase its value in the visible range. For comparison purposes, there have been only a few studies involving TiO_2 and cobalt oxide composite electrodes that have been tested under photoelectrochemical conditions (irradiation, applied potential, *etc*…) close to ours. Qarechallo *et al.* have used a cobalt electrodeposition method onto TiO_2 and they also have reported an increase of the photocurrent by a factor of 2 even if their measured photocurrent is much lower than our results (20 to 40 µA.cm^{-2}).[30] Similar to our results in terms of both relative increase and magnitude, Li *et al.*, observed a photocurrent increase from 100 to 250 µA.cm^{-2} (Xe lamp without AM1.5G filter) when cobalt oxide was deposited by an impregnation/annealing method.[45]

Here, combining (M,N) codoping and cocatalyst deposition, under AM1.5G irradiation allows doubling the photocurrent for (Ta,N) TiO_2-NTs after deposition of CoO-

NPs. For (Nb,N) the photocurrent reaches 0.355 mA.cm^{-2} after deposition, which represents an increase of 2.3 compared to the same sample before decoration. The effect is even more pronounced under visible light for which the current reached 74 µA.cm^{-2} for (Ta,N) TiO_2-NTs (× 3.8) and 141 µA.cm^{-2} for the (Nb,N) TiO_2-NTs (× 5.2) electrodes after CoO deposition. For this last electrode, ~40% of the total photocurrent is generated by visible light photons.

In order to quantitatively assess the photocurrent change induced by the CoO-NPs nanodecoration, the enhancement factors were calculated for all electrodes under solar light ($\varepsilon_{AM1.5}$) and under visible light (ε_{vis}) according to:

$$\varepsilon_{AM1.5} = \frac{J(M,N)_{AM1.5\ w/CoO} - J(M,N)_{AM1.5}}{J(M,N)_{AM1.5}} \times 100 \qquad \text{(eq. 3)}$$

$$\varepsilon_{vis} = \frac{J(M,N)_{Vis\ w/CoO} - J(M,N)_{Vis}}{J(M,N)_{Vis}} \times 100 \qquad \text{(eq. 4)}$$

In these equations $J(M,N)_{AM1.5}$ and $J(M,N)_{AM1.5\ w/CoO}$ are respectively, the photocurrent densities generated, under AM1.5G from the (M,N)-TiO_2-NTs electrodes before and after their decoration with CoO-NPs at 1.0 V vs RHE. ($J(M,N)_{Vis}$ and $J(M,N)_{Vis\ w/CoO}$ in the case of visible light). **Figure S7** shows the variations of $\varepsilon_{AM1.5}$ and ε_{vis} as a function of N_{LP}, which leads to control of the loading of CoO-NPs. For all samples, the PLD of CoO-NPs improves the photon-to-electron conversion efficiency even for the smallest N_{LP} of 500. Under simulated solar light, $\varepsilon_{AM1.5}$ increases with the number of laser pulses from ~20% up to 128% on (Nb,N) TiO_2-NTs and 92% on (Ta,N) TiO_2-NTs (for N_{LP} = 10000). Under visible light irradiation, the improvement of the photocurrent induced by the presence of CoO-NPs is even stronger with ε_{vis} = 426% at N_{LP} = 10000 for (Nb,N) TiO_2-NTs. For similar N_{LP}, the enhancement associated with CoO-NPs deposition is always more important for (Nb,N) codoped samples than (Ta,N) ones.

Table 1: *Photocurrent densities, visible light contribution, and photocurrent enhancement factors for the undoped and (M,N) codoped TiO_2 samples before and after their decoration with CoO-NPs.*

	$J_{AM1.5}$	J_{vis}	*Visible contribution*	$\varepsilon_{AM1.5}$	ε_{vis}	J_{EQE}	$J_{EQE\ vis}$
	mA.cm^{-2}		%	%		mA.cm^{-2}	
TiO_2-NTs	0.137	0.005	3.6	**97**	**204**	0.128	0.008
w/ CoO-NPs (N_{LP}= 2000)	**0.269**	**0.015**	**5.5**			**0.293**	**0.020**
(Nb,N) TiO_2-NTs	0.155	0.027	17.4	**128**	**426**	0.149	0.020
w/ CoO-NPs (N_{LP}= 10000)	**0.355**	**0.141**	**39.8**			**0.341**	**0.144**
(Ta,N) TiO_2-NTs	0.126	0.020	15.9	**92**	**262**	0.136	0.016
w/ CoO-NPs (N_{LP}= 10000)	**0.243**	**0.074**	**30.3**			**0.255**	**0.073**
	±0.005	±0.002	±1.1	±10	±50	±0.010	±0.005

To obtain the spectral response of the modified TiO_2-NTs photoelectrodes, we calculated the EQE of the most representative samples of this study, according to equation 5:

$$EQE(\lambda) = \frac{hc}{e}\left(\frac{J_{ph}(\lambda)}{P(\lambda).\lambda}\right) \qquad \text{(eq.5)}$$

$J_{ph}(\lambda)$ and $P(\lambda)$ are the photocurrent density and incident light power density, at a given wavelength; h is the Planck constant; c is the speed of light and e is the charge of the electron. **Figure 6** shows the measured EQE spectra for TiO_2-NTs, (Nb,N) and (Ta,N) codoped photoelectrodes before and after CoO-NPs deposition. As expected from its band gap of 3.1 eV, the EQE of bare TiO_2-NTs drops to almost zero for wavelengths longer than 400 nm. For the bare (M,N) codoped TiO_2 samples, a small increase of EQE can be seen (inset of **fig. 6)** in the 400-550 nm range. Since this range of wavelength contains most of the energy of the solar spectrum, even if limited, this small increase of charge carrier generation by visible photons can explain the multiplication by a factor 4 of the photocurrent measured by CV in the visible, compared to unmodified TiO_2 electrodes, as shown in **Fig.4** & **Table 1**. After the CoO-NPs deposition, the EQE has more than doubled in the UV region for the pristine TiO_2-NTs, but also increased in the visible, reaching ~1% at 400nm. For the (M,N) codoped samples, the CoO-NPs deposition allows them to double their EQE in the UV part, but it is in the visible part that the strongest enhancement was observed. Indeed, the EQE (at 400 nm)

increased from 1% (before CoO decoration) to 4.1% and 8.4% (after CoO deposition) for (Ta,N) and (Nb,N) codoped TiO_2-NTs, respectively.

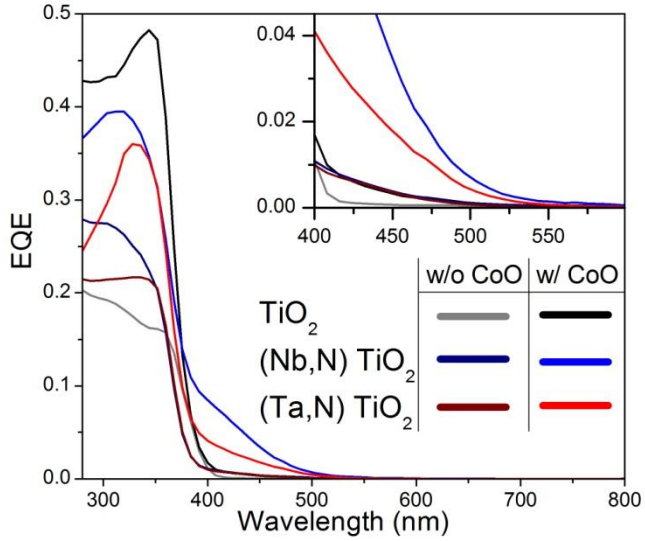

Figure 6: *External quantum efficiency spectra for the undoped and (M,N) codoped TiO_2 electrodes before and after their decoration with CoO-NPs (N_{LP} = 2000 for TiO_2-NTs; N_{LP} = 10000 for (Nb,N) and (Ta,N) TiO_2-NTs).*

The consistency between the data obtained by EQE and those derived from cyclic voltammetry was checked by calculating the theoretical photocurrent J_{EQE} by integrating the EQE convolved with the spectral distribution of the lamp used for CV:

$$J_{EQE} = \frac{e}{h \cdot c} \int_{\lambda_{min}}^{\lambda_{max}} EQE(\lambda) P_{Lamp}(\lambda) \lambda \cdot d\lambda \qquad \text{(eq. 6)}$$

In eq. 6, $P_{Lamp}(\lambda)$ is the spectral distribution of the Xe lamp with AM1.5G filter (or with the 400 nm long pass filter). The calculated values of J_{EQE} (last two columns in **Table 1**) are found in fairly good agreement with the ones from CV. For (Nb,N) TiO_2-NTs decorated with CoO NPs the integration of EQE results is consistent with the fact that 40% of the photocurrent measured by CV originates from visible light-generated electrons.

3.3.Discussion and interpretation of PEC measurements

The PEC measurements indicate that before CoO-NPs deposition, all samples have photocurrent under simulated solar light in the same range, but for (M,N) codoped TiO_2 samples more than 15% of this photocurrent comes from visible photons. After CoO-NPs decoration, all samples saw their efficiencies at least doubling under simulated solar irradiation. Moreover, the enhancement after CoO NPs decoration is even more significant in the visible part of the spectrum, especially for (Nb,N) and (Ta,N) codoped samples with efficiencies in the visible multiplied by 5.3 and 3.6 respectively. To understand the results obtained for photoelectrodes combining TiO_2 codoping and cocatalyst deposition, it is necessary to discuss the changes induced by each approach, how they interact, and how they affect the PEC reaction mechanism.

A first explanation of the enhancement in photocurrent after deposition is a faster charge transfer at the SC/electrolyte interface mediated by the co-catalyst. This effect has been demonstrated by our group and others in the case of CoO or NiO co-catalytic NPs.[30,31,33] Electrochemical impedance spectroscopy has shown that in the case of TiO_2-NTs, the transfer constant becomes faster as the loading of CoO increases (**Figure S8**). This improved charge transfer is related to the electrochemical properties of the SC/cocatalyst/electrolyte interface and should be independent of the illumination wavelength. Nevertheless, the EQE results in Figure 6 and the values of Table 1 revealed that the enhancement is stronger in the spectral range of 400-500 nm. This can be explained by an additional effect observed when CoO-NPs are used as a cocatalyst, namely their direct contribution to the photocurrent due to their p-type semiconducting nature.[30,33] With a bandgap of 2.4-2.5 eV, this contribution of CoO is located at wavelengths below 500 nm and is overlapped with the visible contribution of (M,N) codoping.

The enhancement of photocurrent in the visible part of the spectrum, compared to the overall improvement with the whole solar spectrum (ε_{vis} & $\varepsilon_{AM1.5}$ in Table 1), is particularly noticeable in the case of the decorated (M,N) codoped TiO_2 materials. To separate the different contributions to the visible photocurrent (*i.e.* charge transfer enhancement by the cocatalyst; visible charge generation due to codoping; charge photogeneration in CoO-NPs), we measured the visible photocurrent generated by CoO-NPs deposited at N_{LP} = 10000 on undoped TiO_2-NTs. By subtracting this 33 $\mu A.cm^{-2}$ of photocurrent generated in the CoO NPs from J_{vis} of the (M,N) TiO_2-NTs decorated with CoO (*i.e.* 141 and 74 $\mu A.cm^{-2}$ for (Nb,N) and (Ta,N) respectively) and by comparing these values to J_{vis} before decoration, the photocurrent resulting from the charge transfer enhancement by co-catalyst deposition can be estimated. The calculation indicates that the number of visible photogenerated electrons extracted from the codoped samples is increased by 4-fold for (Nb,N) TiO_2-NTs and 2-fold for (Ta,N) TiO_2-NTs after depositing CoO. This efficiency improvement could be explained by changes in the electronic band structure at the SC/co-catalyst/electrolyte triple phase interface (TPI). The CoO-NPs could modify locally the electronic band energy to favor the collection of h^+ photogenerated in the SC (pinch-off effect)[46] and their transfer to the electrolyte for the OER. The relative positions of the energy levels of the materials constituting the TPI will determine the extent of this phenomenon. For (M,N) codoped TiO_2, while a reduction of the band gap has been observed, the band structure, and in particular the position of its conduction and valence bands (CB and VB), remains largely unknown experimentally. Nakata *et al.* reported an increase of 0.8 eV of the VB energy for Ta,N codoped TiO_2 NPs, lowering the driving force of photogenerated h^+ towards the OER reaction.[47] This reduced energy difference between OER and VB in the case of codoped materials can be indirectly observed on the polarization curves determined from CV (Fig. 5): one can notice that the onset of photocurrent waves for (Nb,N) and (Ta,N) codoped samples (measured at 10 $\mu A.cm^{-}$

^{2}) are shifted of 0.25 and 0.22 V toward more positive potentials respectively, compared to TiO_2. This reduced energy difference between OER and VB could particularly affect h^+ originating from visible light photons, which have an energy close to the VB top and it may explain the low value of EQE for (M,N) codoped samples in the visible region while the UV visible spectroscopy revealed a significant light absorption. After CoO deposition, this increase of onset potential is limited to 0.16 and 0.19 V for (Nb,N) and (Ta,N) codoped samples, indicating an improvement of the SC/electrolyte charge transfer mediated by the cocatalyst. Taken together, these results demonstrate that the photocurrent generated in the visible for the codoped samples after CoO deposition is greater than the addition of the photocurrent generated by p-type CoO NPs and the one from (M,N) codoping. This synergy can also be explained by a faster transfer, mediated by the CoO-NPs, of h^+ generated by the visible light at the triple SC/catalyst/electrolyte interface as compared to the charge recombination. As the TPI density increases with the N_{LP}, this charge transfer is expected to be enhanced, explaining the observed increase in photoconversion efficiency of our (M,N) codoped photoanodes in the visible range.

A notable difference between pristine and (M,N) codoped TiO_2 is the optimal loading of CoO NPs, which changes from 2000 to 10000 N_{LP}. For TiO_2-NTs, beyond 2000 N_{LP}, the contribution of CoO-NPs to the photocurrent in the visible range increases, but the overall photoconversion was lower, due to the scattering of the incident light by co-catalyst NPs at the TiO_2-NT_S surface. The scattering of small NPs increases rapidly for shorter wavelengths as observed in **Figure S9.** For CoO NPs films deposited by PLD (N_{LPs}=10000) on quartz slides, below 300 nm a large part of the light cannot be transmitted. This scattering can also be observed on EQE curves (Fig. 6), which show a decrease at the lowest wavelengths for all samples after the deposition of CoO NPs. For TiO_2-NTs, the negative impact of scattering is not compensated by the increase of photocurrent generated by CoO NPs beyond 2000 N_{LP},

whereas in the case of (M,N) codoped TiO_2-NTs, the synergistic improvement by the cocatalyst deposition and codoping in the visible region, allows compensating this loss due to scattering in UV.

The formation of TPI seems to play a key role to achieve significant photoconversion of visible light on these nanostructures by the synergy of codoping and CoO decoration. However, all the physicochemical phenomena from both approaches may have a role in the charge transfer mechanism. Advanced analytical methods should be employed to determine the electronic structure of (M,N) TiO_2, which remains largely unknown,[44] and how CoO deposition alters the energy band structure of the SC/cocatalyst/electrolyte TPI.

3.4. Quantification of the produced H_2 and O_2

In order to determine if the observed increase of photo-generated charge carriers is effectively used for water splitting reaction, H_2 and O_2 productions of the most representative samples were measured in operando by gas chromatography (GC) during potentiostatic experiments. **Figure 7.a** shows, the photocurrent densities under AM1.5G illumination for reference TiO_2-NTs electrode, TiO_2-NTs with CoO NPs and (Nb,N) TiO_2-NTs with CoO NPs. To highlight the synergistic effect of codoping and cocatalyst deposition, the results obtained under visible light (λ > 400 nm) for (Nb,N) TiO_2-NTs after deposition of CoO NPs were also added (cyan curves). **Figure 7.b and 7.c** shows the H_2 and O_2 production rates (*$n\ H_2$/$n\ O_2$)* associated with these samples calculated according to:

$$n\ H_2(O_2) = \frac{A_{H2(O2)} \times d}{V_m} \qquad \text{(eq. 7)}$$

In eq. 7, *A* is the concentration of H_2 and O_2, determined by GC, *d* is the flow of carrier gas in the cathodic and anodic compartments of the cell, and V_m is the molar volume of the gas.

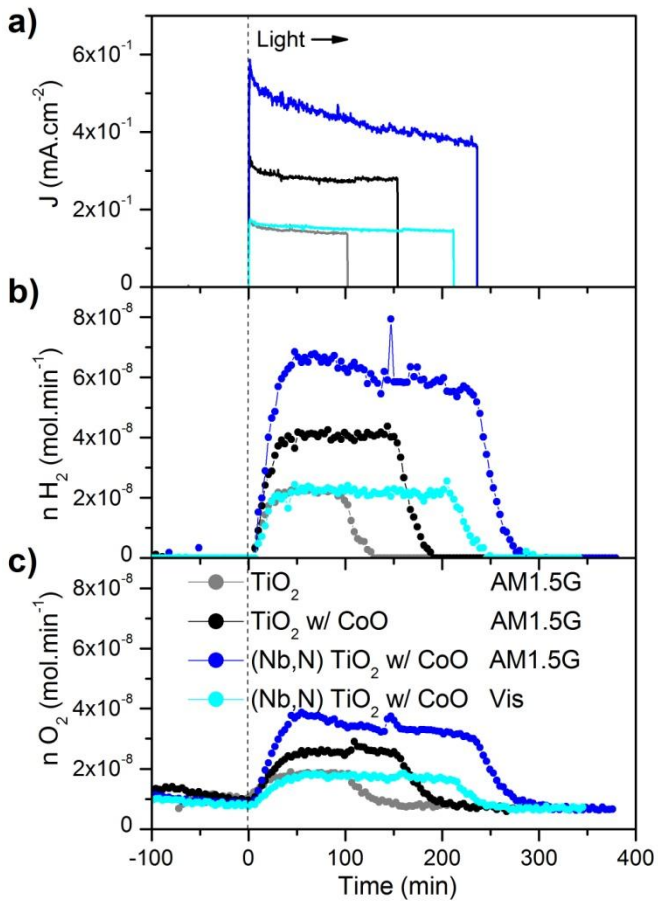

Figure 7: (a) *Photocurrent density generated under AM1.5G by TiO_2-NTs before (grey curves) and after (black) deposition CoO-NPs (N_{LP} = 2000) and (Nb,N) TiO_2-NTs with CoO-NPs (N_{LP} = 10000) under AM1.5G light (blue) and visible light (cyan).* ***(b)*** *and* ***(c)*** *are their associated production rates of H_2 and O_2 gases, respectively, as determined by GC during potentiostatic experiments.*

It can be seen in Figure 7, that the photocurrents for all samples increase and decreases almost immediately when the light is turned on and off while latency is observed for H_2 and O_2 productions. This delay is due to the time required to saturate/desaturate the electrolyte with the photogenerated gases. Consequently, to compare the gas production for the different samples, an average H_2(/O_2) production rate was calculated by integrating $n\ H_2(O_2)$ over the whole experiment duration and dividing it by the illumination time. The obtained average values ($n_{av.}\ H_2$ *and* $n_{av.}\ O_2$) as well as their associated faradic efficiencies for HER ($n_f\ H_2$) and OER ($n_f\ O_2$) are reported **in Table 2**. For the H_2 production, the faradic efficiencies are close to 100% for all samples as expected by using a Pt wire counter electrode. For O_2 production,

the faradic efficiency is 87% for TiO_2-NTs electrode, and probably a part of the photogenerated hole is involved in the generation of other intermediates that cannot be detected by GC such as hydroxyl radicals or hydrogen peroxide. Interestingly, the deposition of CoO-NPs does not increase the faradic efficiency of OER, confirming that CoO cocatalyst role is rather to improve the h^+ collection and their transfer to the electrolyte than playing a catalytic role that would change the selectivity.

Table 2: *Average H_2 and O_2 production rates and faradic efficiencies for the undoped and (Nb,N) codoped TiO_2-NTs samples after their decoration with CoO-NPs. The photocurrent densities measured from CV (J_{CV}) are also reported here for comparison purposes.*

	Irradiation condition	$n_{av.}$ H_2	$n_{av.}$ O_2	Q	J_{CV}	η_f H_2	η_f O_2
		µmol.h^{-1}.cm^{-2}		C.cm^{-2}	mA.cm^{-2}	%	
TiO_2-NTs	AM1.5	2.79	1.20	0.895	0.137	100	87
TiO_2-NTs/ CoO	AM1.5	5.35	2.32	2.610	0.269	100	88
(Nb,N) TiO_2-NTs / CoO	AM1.5	8.18	3.33	6.089	0.355	100	83
	Visible	2.94	1.22	1.942	0.141	100	85
		±0.02	±0.04	±1.10^{-5}	±0.005	±5	±5

The results of gas production, are perfectly in line with the conclusion drawn from the CV and EQE experiments. Thus, in the case of TiO_2-NTs, the deposition of 2000 N_{LP} CoO-NPs allows doubling the hydrogen production rate up to 5.35 µmol.h^{-1}.cm^{-2}. For the (Nb,N) codoped TiO_2-NTs with CoO-NPs decoration, the H_2 production is 3 times higher than pristine TiO_2-NTs. It is worth noting that the hydrogen production of the (Nb,N) TiO_2-NTs with CoO-NPs photoanodes from the sole visible light part exceeds that of bare-TiO_2-NTs irradiated with the full solar spectrum, demonstrating thereby the boost brought by the synergistic effects of codoping and CoO-NPs nanodecoration.

Finally, the stability of the (M,N) codoped TiO_2-NTs after decoration with CoO NPs (N_{LP}=10000) has been investigated, for a minimum of 35 hours under intense UV irradiation (10 mW.cm^{-2}; λ=365 nm), as shown in **figure 8.a**. For both samples, after a slight decrease of the current density during the first 5h (≤ 15%), the photocurrent densities remains stable and

change by only ± 2.5% during the following 30 hours. Figure **8.b**, displays the XPS spectra of the Co 2p before and after PEC tests. The surface ratio Co/(M+Ti) changes only by approximately ± 10%. A slight shift of +0.4 eV for the Co 2p peak can be observed after PEC tests for both the (Ta,N) and (Nb,N) samples, accompanied by a small decrease in the satellite around 787 eV. These two features suggest oxidation of Co^{2+} to Co^{3+} during the test. Nevertheless, the signal after PEC tests is not typical of Co_2O_3 or Co_3O_4, so probably only partial surface oxidation of CoO NPs occurs during the photocatalytic test.[39] The TEM images and elemental cartographies of decorated (Ta,N) TiO_2-NTs before (c,e) and after (d,f) PEC tests are also presented in Figure 8. On the STEM images, the accumulation of cobalt at the surface of the NTs arrays is observed both before and after tests and the average Co concentration in these areas remains around 8% and no changes in the morphology of the CoO nanoparticles were observed by HRTEM. All these analyses comparing the electrodes before and after PEC tests confirm the stability of the (M,N) codoping and the PLD CoO-NPs during at least 35h both in terms of morphology and PEC performances.

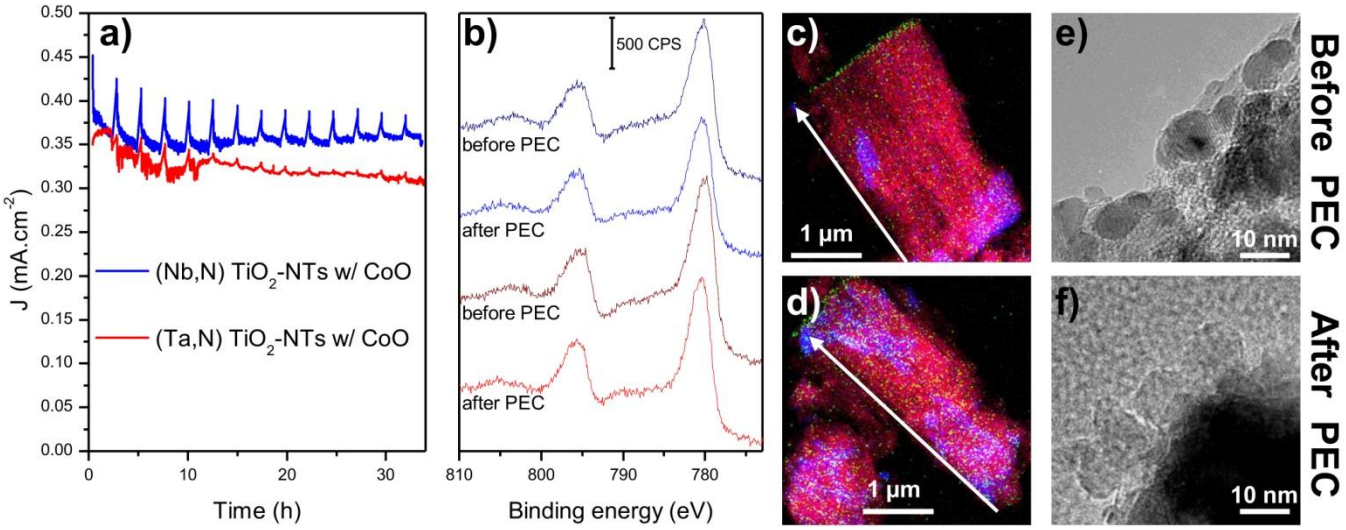

Figure 8: a) *Alternation of cyclic voltammetry and chronoamperometry (E=1.15 V vs RHE; 365nm LED irradiation) of (Nb,N) and (Ta,N) TiO_2-NTs photoanodes after their decoration with CoO nanoparticles (N_{LP}=10000). The spikes observed every two hours are the consequence of an open circuit voltage step between CV and CA experiments.* ***b)*** *High-resolution XPS spectra of Co 2p for CoO decorated (M,N) TiO_2-NTs photoanodes before and after PEC tests.* ***c-f)*** *TEM images of (Ta,N) codoped TiO_2-NTs after their decoration with*

CoO-NPs at N_{LP} = 10000 before (c,e) and after (d,f) PEC tests: ***c,d)*** *STEM EDS mapping of a whole nanotubes films (orientation given by the white arrow; Ti, Ta and Co are represented in red, blue and green respectively);* ***e,f)*** *HRTEM on the upper part of the NTs bunch in figure c) and d) respectively.*

4. Conclusion

In this work (M,N) codoping of TiO_2-NTs (M ≡ Nb or Ta) was combined with nanodecoration by CoO-NPs through the reactive pulsed laser deposition method. Our analyses confirmed that Nb^{5+} and Ta^{5+} are present in the TiO_2-anatase lattice substitution of Ti^{4+}, while N^{3-} anions are present at a concentration below the 1:1 M^{5+}:N^{3-} stoichiometric ratio required for ideal coalloying. Nevertheless, (M,N) codoping of the TiO_2-NTs was found to decrease the optical bandgap of the material, and a photocurrent associated with this low energy transition is observed by EQE. The subsequent nanodecoration of the TiO_2-NTs by CoO-NPs was shown to further improve the PEC performance of all the photoanodes. For pristine TiO_2-NTs, the photocurrent is doubled after CoO-NPs decoration at N_{LP} = 2000, while for (Ta,N) and (Nb,N) codoped samples, the efficiency was found to improve continuously with N_{LP} up to 10000. The strongest enhancement was obtained for the (Nb,N) codoped TiO_2-NTs sample, with a 5-fold increase of the photocurrent in the visible part of the spectrum after decoration with CoO-NPs. For this sample, 40% of the generated photocurrent comes from photons between 400 and 550 nm. Chromatography product quantification confirmed that these photocurrents resulted in H_2 and O_2 productions. The H_2 production associated with visible light (λ > 400 nm) of the (Nb,N) TiO_2-NTs after CoO-NPs deposition with an N_{LP}= 10000, was found to exceed that of pristine TiO_2-NTs under full solar spectrum illumination and their performances remain stable for 35h. The strong PEC boost brought by the combination of both (M,N) codoping and CoO-NPs decoration suggests an important synergistic effect between both approaches. CoO is a p-type SC with a band gap of 2.5 eV

that can provide an additional photocatalytic effect in the visible spectrum. Furthermore, the local modification of the band structure at the TiO_2/CoO/electrolyte TPI plays a key role in improving the charge transfer via the formation of a local p-n heterojunction.

The present work demonstrates the potential of combining (M,N) codoping of TiO_2-NTs and decoration with CoO-NPs to achieve effective and stable nanocomposite photoanodes for visible light conversion. To achieve a better fundamental understanding of the mechanisms behind the boosted PEC performance, more characterizations (such as UPS, PEC Impedance Spectroscopy, etc.) have to be employed to determine accurately the main optoelectronic properties of these complex nanohybrid electrodes.

5. Acknowledgment

The authors gratefully acknowledge the financial support from the Natural Sciences and Engineering Research Council (NSERC) of Canada, and the FRQNT (Fonds de Recherche du Québec Nature et Technologies) of Québec for their financial support. TF is grateful for the joint fellowship obtained from Région Alsace (France) and INRS (Qc, Canada), as well as the GDRI-NMC support for exchanges between France and Québec. This project was partially funded through the ANR BAGETE (ANR-16-CE05-0001-01). The authors would like to thank Thierry Dintzer, Dris Ihiawakrim, Vasiliki Papaefthymiou, Christophe Lefèvre, and Joël Lavoie-Leblanc for their assistance during the SEM, TEM, XPS, XRD, and PLD experiments, respectively. The SEMCro platform is also acknowledged for access to the SEM facility.

6. References

[1] T. Wilberforce, Z. El-Hassan, F.N. Khatib, A. Al Makky, A. Baroutaji, J.G. Carton, A.G. Olabi, Developments of electric cars and fuel cell hydrogen electric cars, International Journal of Hydrogen Energy. 42 (2017) 25695–25734. https://doi.org/10.1016/j.ijhydene.2017.07.054.

[2] C. Acar, I. Dincer, Impact assessment and efficiency evaluation of hydrogen production methods, International Journal of Energy Research. 39 (2015) 1757–1768. https://doi.org/10.1002/er.3302.

[3] M.T. Spitler, M.A. Modestino, T.G. Deutsch, C.X. Xiang, J.R. Durrant, D.V. Esposito, S. Haussener, S. Maldonado, I.D. Sharp, B.A. Parkinson, D.S. Ginley, F.A. Houle, T. Hannappel, N.R. Neale, D.G. Nocera, P.C. McIntyre, Practical challenges in the development of photoelectrochemical solar fuels production, Sustainable Energy Fuels. 4 (2020) 985–995. https://doi.org/10.1039/C9SE00869A.

[4] B.A. Pinaud, J.D. Benck, L.C. Seitz, A.J. Forman, Z. Chen, T.G. Deutsch, B.D. James, K.N. Baum, G.N. Baum, S. Ardo, H. Wang, E. Miller, T.F. Jaramillo, Technical and economic feasibility of centralized facilities for solar hydrogen production via photocatalysis and photoelectrochemistry, Energy Environ. Sci. 6 (2013) 1983. https://doi.org/10.1039/c3ee40831k.

[5] K. Sivula, R. van de Krol, Semiconducting materials for photoelectrochemical energy conversion, Nature Reviews Materials. 1 (2016) 15010. https://doi.org/10.1038/natrevmats.2015.10.

[6] K. Takanabe, Photocatalytic Water Splitting: Quantitative Approaches toward Photocatalyst by Design, ACS Catalysis. 7 (2017) 8006–8022. https://doi.org/10.1021/acscatal.7b02662.

[7] W. Yang, R.R. Prabhakar, J. Tan, S.D. Tilley, J. Moon, Strategies for enhancing the photocurrent, photovoltage, and stability of photoelectrodes for photoelectrochemical water splitting, Chem. Soc. Rev. 48 (2019) 4979–5015. https://doi.org/10.1039/C8CS00997J.

[8] J.H. Kim, D. Hansora, P. Sharma, J.-W. Jang, J.S. Lee, Toward practical solar hydrogen production – an artificial photosynthetic leaf-to-farm challenge, Chem. Soc. Rev. 48 (2019) 1908–1971. https://doi.org/10.1039/C8CS00699G.

[9] Y. Yuan, R. Guo, L. Hong, X. Ji, Z. Lin, Z. Li, W. Pan, A review of metal oxide-based Z-scheme heterojunction photocatalysts: actualities and developments, Materials Today Energy. 21 (2021) 100829. https://doi.org/10.1016/j.mtener.2021.100829.

[10] A. Meng, L. Zhang, B. Cheng, J. Yu, Dual Cocatalysts in TiO_2 Photocatalysis, Adv. Mater. (2019) 1807660. https://doi.org/10.1002/adma.201807660.

[11] R. Long, N.J. English, Band gap engineering of (N,Ta)-codoped TiO_2: A first-principles calculation, Chemical Physics Letters. 478 (2009) 175–179. https://doi.org/10.1016/j.cplett.2009.07.084.

[12] W.-J. Yin, H. Tang, S.-H. Wei, M.M. Al-Jassim, J. Turner, Y. Yan, Band structure engineering of semiconductors for enhanced photoelectrochemical water splitting: The case of TiO_2, Physical Review B. 82 (2010). https://doi.org/10.1103/PhysRevB.82.045106.

[13] J.J. Brancho, B.M. Bartlett, Challenges in Co-Alloyed Titanium Oxynitrides, a Promising Class of Photochemically Active Materials, Chemistry of Materials. 27 (2015) 7207–7217. https://doi.org/10.1021/acs.chemmater.5b02357.

[14] K. Pomoni, A. Vomvas, Chr. Trapalis, Dark conductivity and transient photoconductivity of nanocrystalline undoped and N-doped TiO_2 sol–gel thin films, Thin Solid Films. 516 (2008) 1271–1278. https://doi.org/10.1016/j.tsf.2007.05.040.

[15] D. Zhang, X. Ma, H. Zhang, Y. Liao, Q. Xiang, Enhanced photocatalytic hydrogen evolution activity of carbon and nitrogen self-doped TiO_2 hollow sphere with the creation of oxygen vacancy and Ti3+, Materials Today Energy. 10 (2018) 132–140. https://doi.org/10.1016/j.mtener.2018.08.018.
[16] K. Rajeshwar, A. Thomas, C. Janáky, Photocatalytic Activity of Inorganic Semiconductor Surfaces: Myths, Hype, and Reality, The Journal of Physical Chemistry Letters. 6 (2015) 139–147. https://doi.org/10.1021/jz502586p.
[17] T.M. Breault, B.M. Bartlett, Composition Dependence of TiO_2 :(Nb,N)-*x* Compounds on the Rate of Photocatalytic Methylene Blue Dye Degradation, The Journal of Physical Chemistry C. 117 (2013) 8611–8618. https://doi.org/10.1021/jp312199t.
[18] T.M. Breault, J.J. Brancho, P. Guo, B.M. Bartlett, Visible Light Water Oxidation Using a Co-Catalyst Loaded Anatase-Structured $Ti_{1-(5\,x\,/4)}\ Nb_x\ O_{2-y-\delta}\ N_y$ Compound, Inorganic Chemistry. 52 (2013) 9363–9368. https://doi.org/10.1021/ic400932m.
[19] T. Cottineau, N. Béalu, P.-A. Gross, S.N. Pronkin, N. Keller, E.R. Savinova, V. Keller, One step synthesis of niobium doped titania nanotube arrays to form (N,Nb) co-doped TiO_2 with high visible light photoelectrochemical activity, Journal of Materials Chemistry A. 1 (2013) 2151. https://doi.org/10.1039/c2ta00922f.
[20] R. Pandiyan, N. Delegan, A. Dirany, P. Drogui, M.A. El Khakani, Probing the Electronic Surface Properties and Bandgap Narrowing of in situ N, W, and (W,N) Doped Magnetron-Sputtered TiO_2 Films Intended for Electro-Photocatalytic Applications, The Journal of Physical Chemistry C. 120 (2016) 631–638. https://doi.org/10.1021/acs.jpcc.5b08057.
[21] S. Komtchou, N. Delegan, A. Dirany, P. Drogui, D. Robert, M.A. El Khakani, Photo-electrocatalytic oxidation of atrazine using sputtured deposited TiO_2: WN photoanodes under UV/visible light, Catalysis Today. 340 (2020) 323–333. https://doi.org/10.1016/j.cattod.2019.04.067.
[22] T. Favet, D. Ihiawakrim, V. Keller, T. Cottineau, Anions and cations distribution in M^{5+} /N^{3-} co-alloyed TiO_2 nanotubular structures for photo-electrochemical water splitting, Materials Science in Semiconductor Processing. 73 (2018) 22–29. https://doi.org/10.1016/j.mssp.2017.05.018.
[23] N. Delegan, R. Pandiyan, S. Johnston, A. Dirany, S. Komtchou, P. Drogui, M.A. El Khakani, Lifetime Enhancement of Visible Light Induced Photocharges in Tungsten and Nitrogen *in situ* Codoped TiO_2 :WN Thin Films, J. Phys. Chem. C. 122 (2018) 5411–5419. https://doi.org/10.1021/acs.jpcc.7b11266.
[24] N. Delegan, R. Pandiyan, T. Teranishi, S. Komtchou, A. Dirany, P. Drogui, M.A. El Khakani, Defect engineering of codoped visible light photosensitized TiO_2:WN thin-films for efficient electro-photocatalysis, Journal of Alloys and Compounds. 833 (2020) 155023. https://doi.org/10.1016/j.jallcom.2020.155023.
[25] B.A.D. Williamson, J. Buckeridge, N.P. Chadwick, S. Sathasivam, C.J. Carmalt, I.P. Parkin, D.O. Scanlon, Dispelling the Myth of Passivated Codoping in TiO_2, Chem. Mater. 31 (2019) 2577–2589. https://doi.org/10.1021/acs.chemmater.9b00257.
[26] R. Pittkowski, P. Krtil, J. Rossmeisl, Rationality in the new oxygen evolution catalyst development, Current Opinion in Electrochemistry. 12 (2018) 218–224. https://doi.org/10.1016/j.coelec.2018.11.014.
[27] M. Tahir, L. Pan, F. Idrees, X. Zhang, L. Wang, J.-J. Zou, Z.L. Wang, Electrocatalytic oxygen evolution reaction for energy conversion and storage: A comprehensive review, Nano Energy. 37 (2017) 136–157. https://doi.org/10.1016/j.nanoen.2017.05.022.
[28] C.C.L. McCrory, S. Jung, I.M. Ferrer, S.M. Chatman, J.C. Peters, T.F. Jaramillo, Benchmarking Hydrogen Evolving Reaction and Oxygen Evolving Reaction

Electrocatalysts for Solar Water Splitting Devices, J. Am. Chem. Soc. 137 (2015) 4347–4357. https://doi.org/10.1021/ja510442p.
[29] S. Pokrant, S. Dilger, S. Landsmann, M. Trottmann, Size effects of cocatalysts in photoelectrochemical and photocatalytic water splitting, Materials Today Energy. 5 (2017) 158–163. https://doi.org/10.1016/j.mtener.2017.06.005.
[30] S. Qarechalloo, N. Naseri, F. Salehi, A.Z. Moshfegh, Simply tuned and sustainable cobalt oxide decorated titania nanotubes for photoelectrochemical water splitting, Applied Surface Science. 464 (2019) 68–77. https://doi.org/10.1016/j.apsusc.2018.09.014.
[31] X. Deng, H. Zhang, Q. Ma, Y. Cui, X. Cheng, X. Li, M. Xie, Q. Cheng, Fabrication of p-NiO/n-TiO_2 nano-tube arrays photoelectrode and its enhanced photocatalytic performance for degradation of 4-chlorphenol, Separation and Purification Technology. 186 (2017) 1–9. https://doi.org/10.1016/j.seppur.2017.04.052.
[32] T. Favet, V. Keller, T. Cottineau, M.A. El Khakani, Enhanced visible-light-photoconversion efficiency of TiO_2 nanotubes decorated by pulsed laser deposited CoNi nanoparticles, International Journal of Hydrogen Energy. (2019) S0360319919331970. https://doi.org/10.1016/j.ijhydene.2019.08.179.
[33] T. Favet, T. Cottineau, V. Keller, M.A. El Khakani, Comparative study of the photocatalytic effects of pulsed laser deposited CoO and NiO nanoparticles onto TiO_2 nanotubes for the photoelectrochemical water splitting, Solar Energy Materials and Solar Cells. 217 (2020) 110703. https://doi.org/10.1016/j.solmat.2020.110703.
[34] I. Ka, B. Gonfa, V. Le Borgne, D. Ma, M.A. El Khakani, Pulsed Laser Ablation Based Synthesis of PbS-Quantum Dot-Decorated One-Dimensional Nanostructures and Their Direct Integration into Highly Efficient Nanohybrid Heterojunction-Based Solar Cells, Adv. Funct. Mater. 24 (2014) 4042–4050. https://doi.org/10.1002/adfm.201304191.
[35] A. Imbrogno, R. Pandiyan, M. Barberio, A. Macario, A. Bonanno, M.A. El Khakani, Pulsed-laser-ablation based nanodecoration of multi-wall-carbon nanotubes by Co-Ni nanoparticles for dye-sensitized solar cell counter electrode applications, Mater. Renew. Sustain. Energy. 6 (2017) 11. https://doi.org/10.1007/s40243-017-0095-3.
[36] I. Ka, V. Le Borgne, K. Fujisawa, T. Hayashi, Y.A. Kim, M. Endo, D. Ma, M.A. El Khakani, PbS-quantum-dots/double-wall-carbon-nanotubes nanohybrid based photodetectors with extremely fast response and high responsivity, Materials Today Energy. 16 (2020) 100378. https://doi.org/10.1016/j.mtener.2019.100378.
[37] T. Teranishi, Y. Yoshikawa, J. Leblanc-Lavoie, N. Delegan, I. Ka, A. Kishimoto, M.A. El Khakani, Capacity retention improvement of $LiCoO_2$ cathodes via their laser-ablation-based nanodecoration by $BaTiO_3$ nanoparticles, Journal of Applied Physics. 131 (2022) 124105. https://doi.org/10.1063/5.0075970.
[38] F. Gelb, Y.-C. Chueh, N. Sojic, V. Keller, D. Zigah, T. Cottineau, Electrosynthesis of gradient TiO_2 nanotubes and rapid screening using scanning photoelectrochemical microscopy, Sustainable Energy Fuels. 4 (2020) 1099–1104. https://doi.org/10.1039/C9SE00895K.
[39] B. Qiu, W. Guo, Z. Liang, W. Xia, S. Gao, Q. Wang, X. Yu, R. Zhao, R. Zou, Fabrication of Co_3O_4 nanoparticles in thin porous carbon shells from metal–organic frameworks for enhanced electrochemical performance, RSC Adv. 7 (2017) 13340–13346. https://doi.org/10.1039/C6RA28296B.
[40] G.M. Ingo, S. Dirè, F. Babonneau, XPS studies of SiO_2 TiO_2 powders prepared by sol gel process, (1993).
[41] A. Kubacka, G. Colón, M. Fernández-García, Cationic (V, Mo, Nb, W) doping of TiO_2–anatase: A real alternative for visible light-driven photocatalysts, Catalysis Today. 143 (2009) 286–292. https://doi.org/10.1016/j.cattod.2008.09.028.

[42] G. Liu, K. Wang, N. Hoivik, H. Jakobsen, Progress on free-standing and flow-through TiO_2 nanotube membranes, Solar Energy Materials and Solar Cells. 98 (2012) 24–38. https://doi.org/10.1016/j.solmat.2011.11.004.
[43] J.M. Macak, S.P. Albu, P. Schmuki, Towards ideal hexagonal self-ordering of TiO_2 nanotubes, Physica Status Solidi (RRL) – Rapid Research Letters. 1 (2007) 181–183. https://doi.org/10.1002/pssr.200701148.
[44] S. Khan, T. Lemes Ruwer, N. Khan, A. Köche, R.W. Lodge, H. Coelho-Júnior, R.L. Sommer, M.J. Leite Santos, C.F. Malfatti, C.P. Bergmann, J.A. Fernandes, Revealing the true impact of interstitial and substitutional nitrogen doping in TiO_2 on photoelectrochemical applications, J. Mater. Chem. A. 9 (2021) 12214–12224. https://doi.org/10.1039/D0TA11494D.
[45] S. Li, L. Hou, L. Zhang, L. Chen, Y. Lin, D. wang, T. Xie, Direct evidence of the efficient hole collection process of the CoO_x cocatalyst for photocatalytic reactions: a surface photovoltage study, J. Mater. Chem. A. 3 (2015) 17820–17826. https://doi.org/10.1039/C5TA04653J.
[46] G. Loget, Water oxidation with inhomogeneous metal-silicon interfaces, Current Opinion in Colloid & Interface Science. 39 (2019) 40–50. https://doi.org/10.1016/j.cocis.2019.01.001.
[47] A. Nakada, O. Ishitani, K. Maeda, Solar-driven Z-scheme water splitting using tantalum/nitrogen codoped rutile titania nanorod as an oxygen evolution photocatalyst, J. Mater. Chem. A. 5 (2017) 11710–11719. https://doi.org/10.1039/C6TA10541F.
[48] V. Ramakrishnan, H. Kim, J. Park, B. Yang, Cobalt oxide nanoparticles on TiO_2 nanorod/FTO as a photoanode with enhanced visible light sensitization, RSC Adv. 6 (2016) 9789–9795. https://doi.org/10.1039/C5RA23200G.